

Chapter 2

Cryogenic Properties of Polymer Materials

Shao-Yun Fu

Contents

2.1 Cryogenic Tensile Properties	10
2.2 Cryogenic Shear Strength	20
2.3 Cryogenic Impact Strength and Fracture Toughness	21
2.4 Cryogenic Thermal Properties	24
2.5 Cryogenic Creep and Sliding Performance	27
2.6 Cryogenic Dielectric Properties	30
2.7 Influence of Water Absorption and Cryogenic Aging on Cryogenic Properties	31
2.8 Concluding Remarks and Outlooks	36
References	37

Abstract The cryogenic properties of polymer materials have received great attention with new developments in space, superconducting, electronic and defense technologies as well as large cryogenic engineering projects such as International Thermonuclear Experimental Reactor (ITER), etc. Polymer materials developed for these applications are mainly employed as electrical insulators, thermal insulators, vacuum sealants, and matrix materials for composites used in cryogenic environments. The requirements are extremely severe and complicated for polymer materials in these unique applications. The polymer materials need to possess good mechanical and physical properties at cryogenic temperatures such as liquid helium (4.2 K), liquid hydrogen (20 K), liquid nitrogen (77 K), and liquid oxygen (90 K) temperatures, etc., to meet the high requirements by the cryogenic engineering applications. Herein the cryogenic mechanical and physical properties of polymer materials will be highlighted in this chapter. Cryogenic tensile properties/behaviors are first presented in some details for various neat polymers and filled polymers. Cryogenic shear strength, impact strength, and fracture toughness are then

S.-Y. Fu (✉)

Technical Institute of Physics and Chemistry, Chinese Academy of Sciences,
Beijing 100190, China
e-mail: syfu@mail.ipc.ac.cn

discussed. Afterwards, cryogenic thermal, creep, sliding, and dielectric properties of polymers are briefly summarized. Finally, discussions about effects of water absorption and cryogenic aging on cryogenic properties of some polymers are conducted.

Keywords Polymers • Nanocomposites • Cryogenic mechanical properties • Cryogenic physical properties • Low temperatures • Cryogenic engineering

2.1 Cryogenic Tensile Properties

Polymers have wide applications in various industries and also in cryogenic engineering-related areas. Cryogenic mechanical properties of polymers are important parameters for their successful applications in extremely low temperature environments. For example, in a fiber-reinforced polymer composite, since the internal stresses will be generated as a result of the unequal coefficients of thermal expansion between fibers and matrix, the micro-cracking of the polymer matrix may take place when temperature is decreased down to cryogenic temperature [1]. Sometimes even fracture of the polymer matrix can occur if the thermal stress-induced stress intensity factor exceeds the fracture toughness of polymers [2]. The cryogenic mechanical properties including strength, modulus, ductility, fracture resistance, creep, and sliding performance, etc., of polymers play a critical role in determining their applicability in cryogenic engineering environments. Tensile behaviors at cryogenic temperatures are first discussed below for various polymers and nanocomposites.

Some polymers, that exhibit good mechanical properties at cryogenic temperatures, are studied by focusing on their cryogenic tensile behaviors. Cryogenic tensile tests are performed on aromatic polyimide films (Upilex-R and Upilex-S), which are the products of polycondensation reactions between biphenyl-tetracarboxylic dianhydride (BPDA) and various diamines, and a polypyromellitimide (PPMI)-designated Kapton film [3]. Figure 2.1 displays stress-strain curves for Upilex-R and -S films as well as Kapton film at 77 K. Although the main chains contain the BPDA moiety as a common structural unit, the tensile behaviors of the two Upilexs at 77 K are largely affected by the molecular structure of the diamine moieties. Upilex-R retains considerable ductility but exhibits much lower yield stress around 250 MPa at 77 K. In contrast, Upilex-S withstands elongations in excess of 10 % at a much higher stress level of about 500 MPa at 77 K. The stress-strain curve of Kapton film at 77 K is located between those of the two Upilexs. These observations indicate that aromatic polyimide films exhibit good mechanical properties at cryogenic temperatures.

For semicrystalline polymers, the degree of crystallinity exhibits an effect on their tensile properties at cryogenic temperatures. Figure 2.2 shows the results of tensile tests at 77 K for some biaxially stretched polyethylene-2,6-naphthalenedicarboxylate (PEN) films with different degrees of crystallinity, which is the condensation product from 2,6-naphthalenedicarboxylic acid and ethylene glycol [3].

Fig. 2.1 Stress-strain curves at 77 K for Upilex-R, Upilex-S, and Kapton films [3]

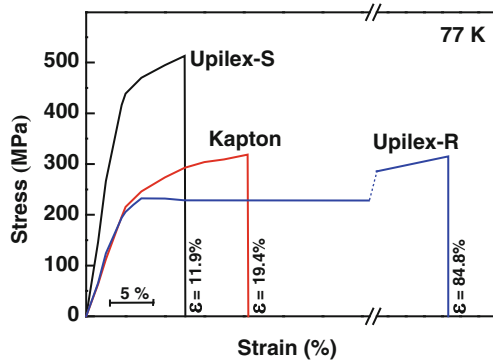
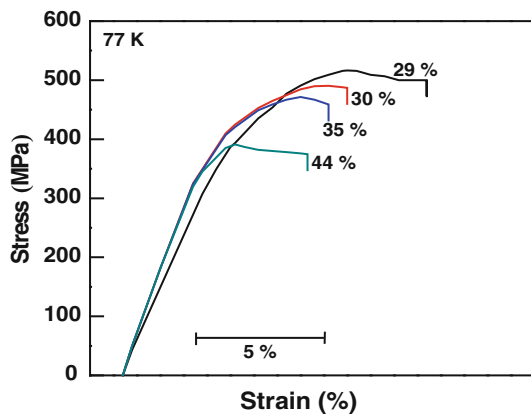


Fig. 2.2 Stress-strain curves at 77 K for biaxially stretched PEN films with various degrees of crystallinity [3]. The crystallinity degree data are shown in the figure



It appears that the strength and the elongation at break of PEN films decreases with increasing the degree of crystallinity.

Figure 2.3 exhibits the stress-strain curves of polyphenylene sulfide (PPS) film at different temperatures. The curve at RT (300 K) is typical of hard ductile polymers and shows a gradual increase in strength beyond the elastic limit. This feature remains unchanged with decreasing temperature from RT to 4.2 K. This indicates that no transition region from ductile to brittle exists between 300 and 4.2 K. Table 2.1 presents the results for the mechanical properties of PPS film at four different temperatures obtained from Fig. 2.3. Both the tensile strength and the tensile modulus gradually increase with decreasing temperature. And the elongation at break remarkably decreases with the decrease in temperature. Nonetheless, the PPS film still retains some ductility even at a very low temperature of 4.2 K.

The effect of crystallinity degree on the tensile properties is exhibited in Fig. 2.4 for the (002) plane of drawn and annealed poly(trimethylene terephthalate) (PTT) film at 18 and 300 K [4]. The results are for the drawn film (crystallinity $\chi_c = 20.2\%$) and those for the drawn (draw ratio = 4) and annealed (for 30 min at 473 K) PPT film ($\chi_c = 41\%$) at 300 K. The inclination of the line corresponds to the crystal modulus of 2.59 GPa along the chain axis. Though the drawn film and

Fig. 2.3 Stress-strain curves at different temperatures for PPS film [3]

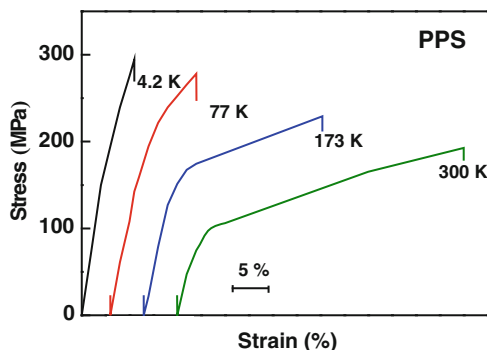


Table 2.1 Tensile properties of the polyphenylene sulfide (PPS) film at RT and cryogenic temperatures [3]

Temperature (K)	Tensile strength (MPa)	Tensile modulus (GPa)	Elongation at break (%)
4.2	295	5.2	7.9
77	260	4.8	12.2
173	215	4.2	22.8
RT (300)	188	3.8	38.2

the drawn-and-annealed film have different microstructures, their identical modulus values at 300 K are strong evidence that the stress distribution in PTT film is homogeneous. At 18 K the measured strain vs. stress gives a straight line through the origin, the slope of which corresponds to a modulus of 5.39 GPa, more than twice the modulus of PTT film at 300 K. This indicates that the modulus value of PTT film is strongly dependent on testing temperature.

Figure 2.5 exhibits the stress-strain curves of the drawn PTT film under cyclic loads at 300 and 18 K. The loading and unloading curves obtained at 300 K show hysteresis loops, but those obtained at 18 K coincide with one another up to 8 %. It is reported that the elongation at break of some polyimides is more than 10 % at 77 K [3]. Nonetheless, polyimides deform with yielding at the strain less than 5 %, after which plastic deformation is observed. Therefore, PTT film possesses a comparatively higher elasticity up to 8 % at a very low temperature of 18 K.

Addition of montmorillonite (MMT) at proper contents may enhance the cryogenic tensile strength of polyimide film as shown in Table 2.2 [5]. The tensile strength of MMT/polyimide (PI) composite films at 77 K is generally higher than that at room temperature (RT) except at 20 wt.%. This is mainly attributed to: (1) the PI strength becomes higher at 77 K, resulting in a higher composite strength than at RT; (2) the MMT/PI matrix interfacial bonding becomes stronger at 77 K than at RT because of the thermal shrinkage of PI matrix and tight clamping of the MMT by the PI matrix at cryogenic temperature, leading to a higher composite strength. Moreover, when the MMT content is 20 wt.%, the tensile strength at 77 K is dramatically decreased by the addition of MMT and is lower than that at RT. This is mainly due to the aggregations of MMT at a very high MMT content [5], which would prick up the stress concentration more severely at 77 K than at RT at the sites of MMT/PI interfaces.

Fig. 2.4 Stress-strain curves for the (002) plane of drawn and annealed PTT films at (filled square) 18 K and at (open circle) 300 K [4]. Also shown is the plot for the drawn PTT film at 300 K (filled circle)

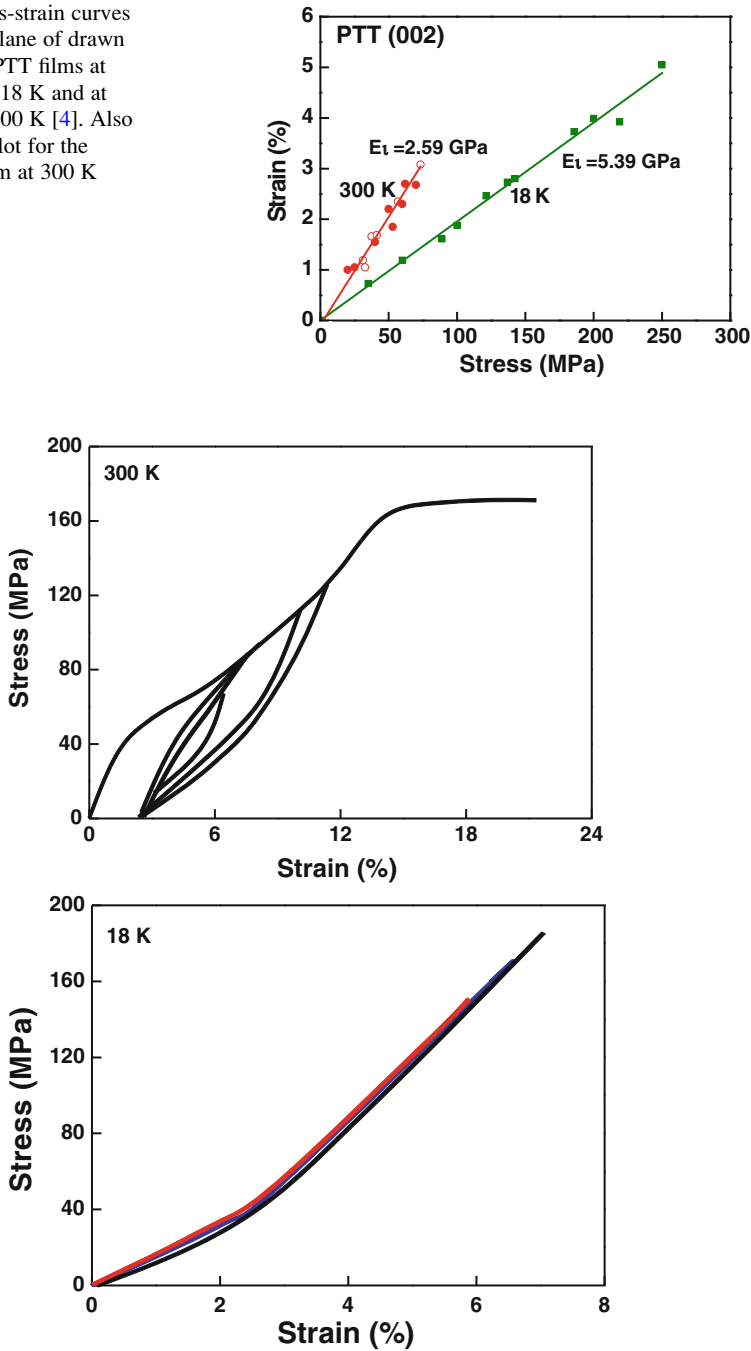


Fig. 2.5 Stress-strain curves of drawn PTT films (draw ratio = 4) under cyclic loads at 300 and 18 K [4]

Table 2.2 The tensile strength of montmorillonite (MMT)/polyimide (PI) composite films at RT and 77 K [5]

MMT content (wt.%)	0	1	3	5	10	20
RT	120	131	120	115	114	84
77 K	188	211	191	158	124	60

Except polymer films as introduced above, epoxy resins are also widely used in cryogenic engineering areas as insulators, vacuum sealants, matrix materials for composites, etc. However, epoxy resins are generally brittle at cryogenic temperatures and residual internal stresses due to thermal cycling may be high to induce fracture of epoxy resins. So, their high cryogenic mechanical properties are very important to assure that epoxy resins can be used under severe cryogenic environments. Therefore, the mechanical properties of epoxy resins at cryogenic temperatures are often enhanced using various modifiers such as carbon nanotubes, thermoplastics, MMT, and other fillers to meet the high requirements by cryogenic engineering applications.

Multi-walled carbon nanotubes (MWCNTs, Showa Denko KK) are used to reinforce a diglycidyl ether of bisphenol-F (DGEBA, DER354) epoxy resin cured with diethyl toluene diamine (DETDA, ETHACURE-100) and modified by a reactive aliphatic diluent (Changshu Jiafa Chemistry Co) [6]. The software SemAfore 4.0 is used on the SEM images of carbon nanotubes to measure the diameter of carbon nanotubes as shown in Fig. 2.6 and the average diameter value is estimated to be about 87 nm for CNTs.

The tensile properties at room temperature and liquid nitrogen temperature (77 K) are studied for the epoxy matrix and epoxy nanocomposites. Table 2.3 shows the results for the tensile properties at RT and 77 K of the epoxy matrix and epoxy nanocomposites [6]. It can be seen from Table 2.3 that the tensile strength of the CNT/epoxy nanocomposites at RT is almost independent of the MWCNT addition. By contrary, a significant enhancement in the cryogenic strength is observed by the addition of MWCNTs at appropriate contents. The cryogenic tensile strength reaches the maximum at the CNT content of 0.5 wt.% and then decreases as the CNT content increases further. Moreover, it is seen from Table 2.3 that the cryogenic strength is consistently higher than the RT strength with the same composition. On the one hand, when the temperature decreases from RT to 77 K, the chemical bond and molecules will shrink and the binding forces between molecules will become strong for the epoxy matrix. Thus, a greater load will be needed to break the epoxy matrix at 77 K, leading to a higher strength of the epoxy matrix at 77 K than at RT. On the other hand, the thermal contraction of the epoxy matrix due to the temperature decrease raises the clamping force to the carbon nanotubes at 77 K, this would lead to a stronger CNT-epoxy interfacial bonding.

When there is a relatively poor bonding between the matrix and the CNTs, CNTs would be easily pulled out with smooth surfaces for the RT case as shown in Fig. 2.7a [6]. The weak bonding leads to poor stress transfer from epoxy matrix to CNTs and the CNTs would then have a low reinforcing efficiency, resulting in the insensitivity of the composite strength to the CNT content. When there is a strong

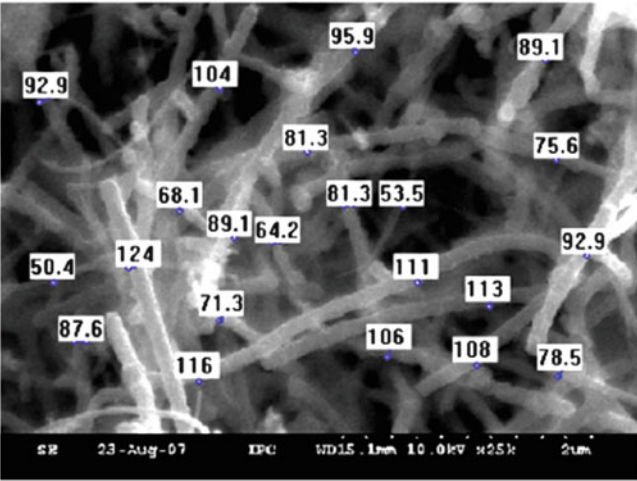


Fig. 2.6 Measurement of the diameters of pristine MWCNTs using the software SemAfore 4.0 [6]

Table 2.3 Tensile properties at RT and 77 K of the epoxy matrix and epoxy nanocomposites [6]

CNT (wt.%)	Tensile strength (MPa)		Tensile modulus (GPa)		Failure strain (%)	
	RT	77 K	RT	77 K	RT	77 K
0	73.4 ± 1.3	92.7 ± 1.1	2.67 ± 0.08	4.58 ± 0.02	4.62 ± 0.31	2.50 ± 0.04
0.02	73.1 ± 1.8	94.8 ± 0.5	2.72 ± 0.05	4.80 ± 0.05	4.71 ± 0.12	2.67 ± 0.03
0.05	72.2 ± 1.6	102.5 ± 2.5	2.77 ± 0.09	4.92 ± 0.08	4.82 ± 0.18	2.82 ± 0.05
0.2	73.1 ± 0.6	116.4 ± 3.4	2.83 ± 0.08	5.02 ± 0.06	4.94 ± 0.13	3.08 ± 0.07
0.5	74.4 ± 1.2	119.4 ± 2.0	3.09 ± 0.02	5.26 ± 0.07	5.04 ± 0.07	3.20 ± 0.05
1	71.5 ± 1.5	112.8 ± 1.5	3.11 ± 0.01	5.49 ± 0.08	4.51 ± 0.19	2.64 ± 0.06
2	68.8 ± 2.3	81.4 ± 3.3	3.13 ± 0.06	5.53 ± 0.04	4.15 ± 0.14	2.20 ± 0.04

bonding between the matrix and the CNTs, the surface of CNTs would be attached with a large amount of epoxy matrix as shown in Fig. 2.7b for the 77 K case [6]. The CNT-epoxy interfacial strength must exceed the yield strength of the epoxy matrix so that the epoxy matrix could be broken and attached on the surface of CNTs. At the relatively high CNT content (2 wt.%), largely aggregated CNTs lead to a slightly lower strength than that of the epoxy matrix because the agglomeration of CNTs for the high CNT content gives rise to weak CNT–polymer interactions and high stress concentrations similar to the case of clay–epoxy composites [7], resulting in the reduction of the tensile strength.

Over 100 measurements are carried out on SEM micrographs as shown in Fig. 2.7 of the fractured surfaces of the samples using the software SemAfore 4.0 to obtain the average CNT diameters [6]. The average diameters of CNTs are estimated to be 93 ± 23 and 180 ± 61 nm, respectively, for the cases of RT and 77 K, confirming that the surfaces of CNTs are quite smooth for the RT case due to relatively weak CNT-epoxy interfacial bonding while are quite rough with matrix attachment for the 77 K case due to strong CNT-epoxy interfacial bonding.

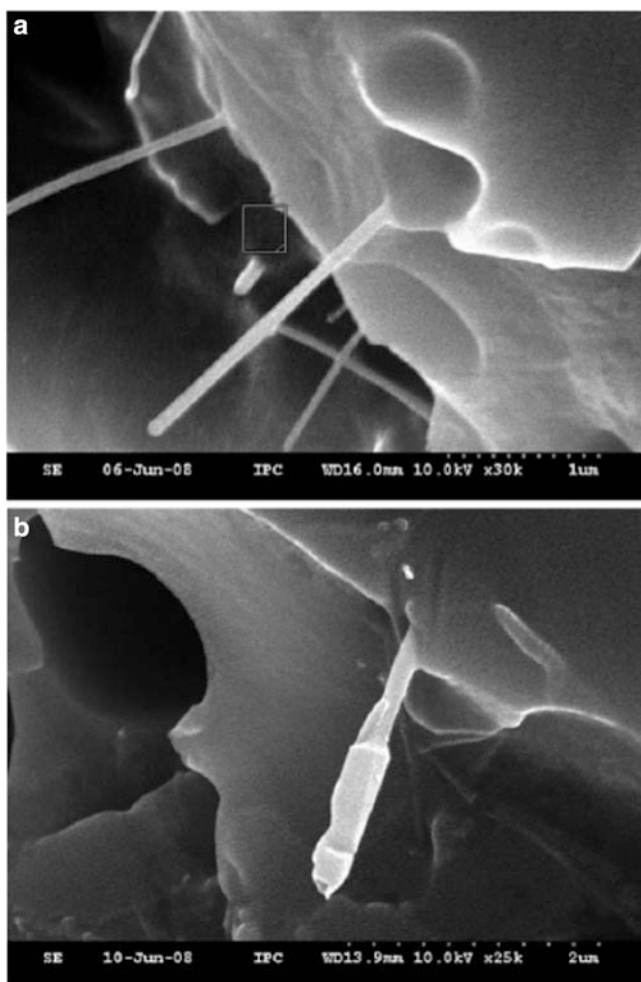


Fig. 2.7 SEM images showing CNT pullout from the tensile fracture surfaces of MWCNT/epoxy composites at (a) RT and (b) 77 K [6]

Similarly, a strong interfacial adhesion between carbon fibers and polyamide matrix is observed at 77 K [8]. A strong CNT-epoxy interfacial bonding would increase the stress transfer from the epoxy matrix to the CNTs and hence enhance the CNT reinforcing efficiency. Consequently, the strength of the epoxy composites is significantly enhanced at 77 K and the cryogenic strength is much higher than at RT.

Table 2.3 also exhibits that Young's modulus of CNT/epoxy composites at both RT and 77 K increases consistently with increasing the CNT content. Moreover, the cryogenic Young's modulus is higher than the RT modulus with the same composition. This is due to the fact that on the one hand, the molecules of epoxy

matrix become stiff due to the restrained mobility of the molecules at 77 K; on the other hand, the CNTs would become stiffer at 77 K than at RT. Finally, in terms of the principles for particulate polymer composites [9] or short fiber-reinforced polymer composites [10, 11], the Young's modulus of the CNT/epoxy composites must be higher at 77 K than at RT.

In addition, it can be seen from Table 2.3 that the failure strain is enhanced by the addition of CNTs at appropriate contents to the epoxy matrix. The epoxy matrix is actually a blend showing a sea-island structure, which is consisted of brittle epoxy phase (DGEBA) and second diluent soft phase [12]. The second soft phase islands are uniformly distributed in the brittle DGEBA phase sea and thus good cryogenic mechanical properties have been achieved [12]. Here, MWCNTs are employed to further improve the cryogenic mechanical properties of brittle DGEBA epoxy resin.

A bisphenol-A diglycidyl ether (DGEBA, CYD-128) is used as the matrix reinforced by MMT and the MMT/epoxy composites are prepared under the ultrasonic treatment [13]. TEM morphologies of the raw MMT, organo-MMT prepared in HCl solution and MMT/epoxy nanocomposites (1 and 3 wt.%) are presented in Fig. 2.8a–d. The size of organo-MMT particles is about 20 nm thick and 200–500 nm long as shown in Fig. 2.8b, which is smaller than that of raw MMT in Fig. 2.8a, especially in thickness. Figure 2.8c exhibits that the organo-MMT has been intercalated and exfoliated in the nanocomposite with the 1 wt.% organo-MMT content. This is because netlike macromolecules form the interlayer of the organo-MMT during the curing process [14]. As the organo-MMT content in the composites is increased to 3 wt.%, the conglomerating probability of organo-MMT and the quantity of non-exfoliated organo-MMT inside the epoxy matrix increase. Thus, it can be seen in Fig. 2.8d that serious aggregations occur at the 3 wt.% organo-MMT content.

Figure 2.9 shows the tensile strength of the MMT/epoxy samples at RT and 77 K as a function of organo-MMT weight content from zero to 3 wt.% and the error bars represent the standard deviation. It can be seen that the organo-MMT content has marginal influence on the tensile strength of MMT/epoxy composites. As the organo-MMT content increases, the tensile strength at both RT and 77 K reaches the maximum at the 0.1 wt.% organo-MMT content. The intercalated and exfoliated organo-MMT layers shown in Fig. 2.8c serve as the short fasciculus inside the composite. The addition of short fasciculus to the epoxy matrix can reinforce the epoxy matrix and contribute to the increase of the tensile strength of the MMT/epoxy composite at the 1 wt.% organo-MMT content. The tensile strength at 77 K is generally higher than that at RT at the same content of organo-MMT due to the two similar major reasons as mentioned for MWCNT/epoxy nanocomposites [6]. The strength of the epoxy matrix becomes higher at 77 K and the interfacial bonding becomes stronger at 77 K than at RT, leading to the higher composite strength.

The tensile modulus of the epoxy composites at RT and 77 K is shown in Fig. 2.10 as a function of organo-MMT content. The tensile modulus increases almost linearly as the organo-MMT content increases. This is mainly because organo-MMT has a higher modulus than epoxy matrix. Moreover, Fig. 2.10

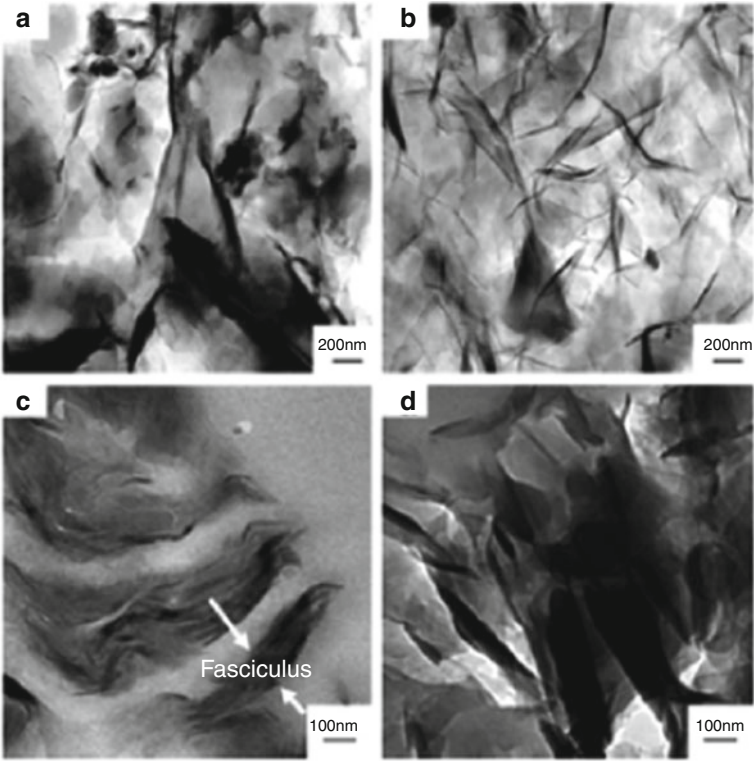
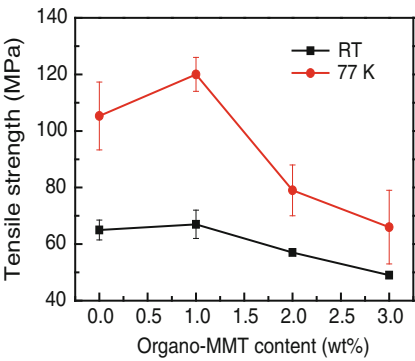


Fig. 2.8 TEM micrographs of (a) raw MMT, (b) organo-MMT, (c) 1 wt.% MMT/epoxy composite, and (d) 3 wt.% MMT/epoxy composite [13]

Fig. 2.9 Effect of organo-MMT content on tensile strength of MMT/epoxy composites at RT and 77 K [13]



displays that the modulus at 77 K is much higher than that at RT at the same organo-MMT content. On the one hand, the modulus of the epoxy matrix at 77 K is higher than that at RT content due to the tight arrangement of polymer molecules. On the other hand, the modulus of MMT would also be higher at 77 K than at room

Fig. 2.10 Effect of organo-MMT content on tensile modulus of MMT/epoxy composites at RT and 77 K [13]

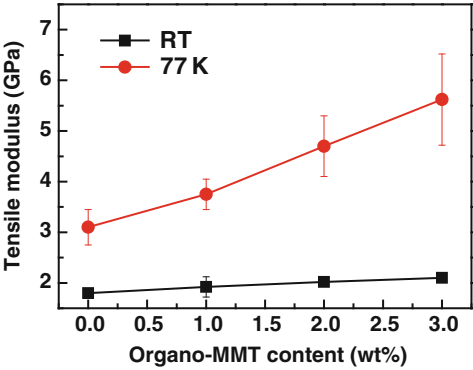


Table 2.4 Material properties of the polycarbonate and the MWCNT/PC composite [15, 16]

Material	Temperature (K)	Yield strength (MPa)	Tensile modulus (GPa)	Poisson's ratio
Polycarbonate	RT	34.0	2.35	0.39
	77 K	92.7	4.50	0.38
Composite	RT	36.8	2.56	0.39
	77 K	104	4.65	0.38

temperature. These two major contributions lead to the higher modulus of the composites at 77 K than at RT.

The tensile properties including yield strength, Young's modulus and Poisson's ratio at RT and 77 K of polycarbonate (PC) and 2.5 wt.% MWCNT/PC composite are given in Table 2.4 [15, 16]. It is clear that yield strength and Young's modulus at 77 K are much higher than those at RT. The Poisson's ratio is almost independent of temperature.

A recent development in polymer nanocomposites is the use of CNTs as a smart nano-filler, in which the CNTs serve as strain or damage sensors [17]. The principle is that the deformation, damage initiation, and evolution of CNT-based composites can result in obvious electrical resistance change. The electrical and mechanical responses of MWCNT/PC composites are recently investigated under tensile loading at 77 K and also RT for the purpose of comparison [15]. The load P and the normalized resistance change $\Delta R/R_0$ are plotted in Fig. 2.11 as a function of displacement δ for the 2.5 wt.% MWCNT/PC composite [15].

It can be seen from Fig. 2.11a that the resistance change is very small in the beginning. The composite has an initial resistance R_0 of 11 k Ω at RT. This small change in resistance is due to the specimen deformation [17]. But significant resistance change takes place around 0.8 mm displacement, which corresponds to the initiation of nonlinear load-displacement response. In addition, during loading of the composite specimen the resistance response and crack length show similar trends. This observation demonstrates that crack propagation results in the electrical resistance change and the resistance monitoring enables the detection of crack initiation and propagation in real-time mode.

Fig. 2.11 Load and normalized resistance change vs. displacement for the MWCNT/PC composite at (a) RT and (b) 77 K [15]

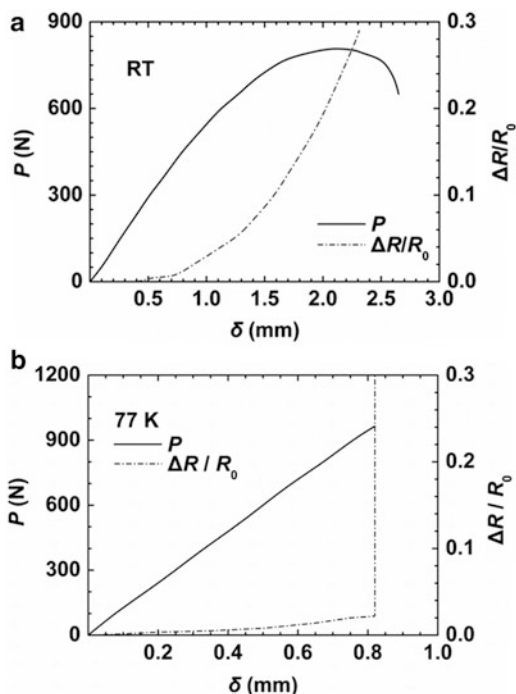


Figure 2.11b shows the load P and the normalized resistance change $\Delta R/R_0$ as a function of displacement δ for the 2.5 wt.% MWCNT/PC composite at 77 K. The initial resistance R_0 at 77 K is 27 k Ω . The load-displacement curve at 77 K exhibits a linear relationship. The resistance-displacement curve displays a small resistance change, similar to the corresponding response at RT. When the maximum load is reached, the sharp increase in resistance takes place. Thus, it can be considered that the crack catastrophically propagates through the specimen at 77 K when the maximum load is reached.

2.2 Cryogenic Shear Strength

Adhesives are required to have good bond strength at cryogenic temperatures for cryogenic engineering applications. Thus, it is of significance to study formulations of adhesive resins with high shear strength at cryogenic temperatures [18, 19].

The cured samples are cycled between liquid nitrogen and ambient condition until failure. The shear strengths of some formulated epoxy resins are listed in Table 2.5. It reveals that the matrix cured by hardener HK-021 has a higher shear strength than that of the NA hardener. Moreover, after blending with multifunctional epoxies, the lap shear strength decreases. When the ratio of multifunctional epoxy is great in the formulation such as formulation 5 mixed with 100-phr

Table 2.5 Lap shear strength of some formulated adhesive resins [18]^a

Formulation no.	Composition	Parts by weight (phr)	Shear strength (MPa)			
			Initial		After 15 cycles	
			RT	77 K	RT	77 K
1	DGEBA	100	6.6	7.1	6.4	6.8
	NA	80				
	A-178 TM	1				
2	DGEBA	100	8.2	9.7	8.3	9.6
	HK-021	80				
	A-178 TM	1				
3	DGEBA	100	5.0	4.5	4.9	4.5
	TGBA	25				
	NA	130				
	A-178 TM	1				
4	DGEBA	100	5.0	6.3	5.0	6.1
	TGDMDA	25				
	NA	150				
	A-178 TM	1				
5	DGEBA	100	5.2	5.2	5.2	5.2
	TGDMDA	100				
	NA	170				
	A-178 TM	1				

^aDGEBA diglycidyl ether of bisphenol A; NA (*hardener*) nadictetrahydric-methylanhydride; HK-021 anhydride hardener based on NA but modified by diol molecule; A-178TM silane coupling agent; TGBA (*multifunctional epoxy*) triglycidyl benzylamine; TGDMDA (*multifunctional epoxy*) tetraglycidyl dibenzmethyldiamine

TGDMDA, its lap shear strength decreases remarkably at RT and even more at 77 K, compared to formulation 1 with 0 phr of TGDMDA and the same hardener.

Hu and Huang also studied the lap shear strength of modified epoxy adhesives by mixing with flexible polyether and blending with multifunctional epoxy [19]. The influences of flexible polyether chain amount in the network of the adhesives and synergetic effect of mixed resins with different functionalities on the shear strength of epoxy adhesives at 77 K and RT are investigated. The lap shear strength increases at RT and 77 K with increasing polyether chain content in the network of the epoxy resin with unique functionality. When the adhesive is a mixture of epoxy resins with multifunctional epoxy, a maximum or a minimum lap shear strength at 77 K can be obtained at certain resin ratio, which depends on that whether the polyether chain is introduced into the network.

2.3 Cryogenic Impact Strength and Fracture Toughness

The fracture resistance of polymers will generally be lowered when temperature decreases from RT to cryogenic temperatures. The brittleness of polymers limits their uses in cryogenic environments. Thus, the cryogenic fracture resistance such

Table 2.6 Fracture resistance of neat resin polymers determined from fracture testing [20]

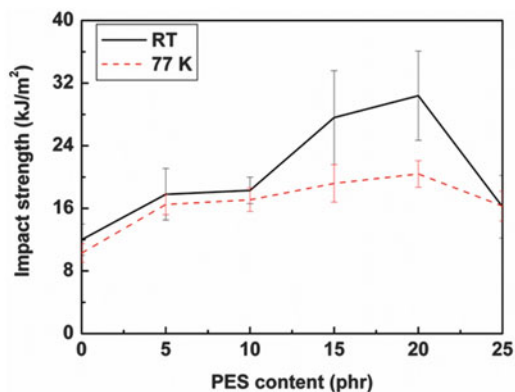
Code	Temperature (K)	K_{IC} (MPa m ^{1/2})	K_{IC} (MPa m ^{1/2})	G_c (kJ/m ²)	G_{IC} (kJ/m ²)
PETI-5	79	6.01	6.01	3.15	3.15
	RT	3.68	3.68	2.98	2.98
	432	3.92	NA	3.60	NA
5050 (plaque 1)	83	7.20	6.49	5.46	4.36
	RT	5.28	5.28	5.89	5.89
	434	4.72	NA	4.20	NA
5050 (plaque 2)	84	7.01	7.01	5.11	5.11
	RT	4.84	4.84	4.97	4.97
	433	4.56	NA	3.90	NA
LCR	84	1.88	1.83	1.38	1.25
	RT	1.45	1.45	1.94	1.94
	433	0.29	NA	1.08	NA

as cryogenic impact strength or cryogenic fracture toughness is a very important parameter for polymers used in extremely low temperature environments. Sometimes brittle polymers such as epoxy resins, etc., are often modified using various modifiers.

Fracture toughness of three polymers (LaRC PETI-5, LaRC 5050, and LCR) manufactured by NASA LaCR is studied [20], where PETI-5 is a phenylethynyl-terminated imide oligomer ($M_n \sim 5,500$ g/mol), LaRC 5050 a thermoplastic aromatic polyimide endcapped with phthalic anhydride of a molecular weight ($M_n \sim 12,000$ g/mol) and a 50:50 ratio of diamine monomers in the backbone making it more flexible while LCR a liquid crystal oligomer with changes from a thermoplastic to a thermoset upon curing. Fracture toughness results for these polymers are shown in Table 2.6. It can be seen from Table 2.6 that the stress intensity factor (K) and fracture energy (G) are dependent on testing temperature. K shows a higher value at cryogenic temperature than at room temperature or high temperature for all samples. G displays different trends for different samples. G exhibits a higher value at cryogenic temperature than at RT but a lower value than at high temperature for PETI-5. For 5050 (plaque 1) and LCR materials, G shows a higher value at cryogenic temperature than at high temperature but a lower value than at RT. On the other hand, for 5050 (plaque 2), G displays the highest value at cryogenic temperature compared to that at RT and high temperature. It should be noted that at high temperature no tests yield valid K_{IC} and G_{IC} results according to the ASTM D 638-01 standard.

The impact strength of epoxy resins modified by poly(ethersulfone) (PES) is studied as a function of PES content [21]. Figure 2.12 shows the dependence of the impact strength at RT and 77 K on the PES content in the cured epoxy resins. The error bars denote the standard deviation. As expected, the impact strength at RT significantly increases with increasing the PES content in the modified epoxy system. An addition of 5 phr PES relative to the epoxy results in about 49 % increase in the impact strength at RT compared to the neat epoxy. This is because that the immiscible PES-rich domains in the modified epoxy system would increase the

Fig. 2.12 Impact strength of the unmodified and modified epoxy resin at RT and 77 K [21]



impact strength through crack trapping and bridging of the dispersed thermoplastics [22, 23]. And the impact strength shows small variation with increasing the PES content from 5 to 10 phr and from 15 to 20 phr because of the similar morphological features developed after curing [21]. A rapid increase in the impact strength can be observed when the PES content increases from 10 to 15 phr (see Fig. 2.12). The impact strength of the PES-modified epoxy is up to the maximum value for the 20 phr case, where a co-continuous phase structure is formed for dispersed PES phase and epoxy main phase [21]. A large decrease in the impact strength is observed when the PES content is further increased to 25 phr, where the PES rich domains form large agglomerates, which act as defects and then initiate failure.

A DGEBA epoxy resin cured by methyltetrahydrophthalic anhydride is modified by a hyperbranched polymer (polyester Boltorn H30), which is a third-generation hyperbranched polyester with 32 primary hydroxyl groups on the shell and it is an amorphous solid at RT. Effects of the H30 content on the impact strength at RT and 77 K of the cured epoxies are shown in Table 2.7 [24]. It exhibits that the RT and cryogenic impact strength increases up to the maximum by adding the 10 wt.% H30 and decreases afterwards with further increasing the H30 content. In general, it is expected that the impact strength of epoxy resins at 77 K should be lower than that at RT since epoxy resins become normally more brittle at low temperatures. Here it is interesting to note that the impact strength at 77 K of the modified epoxy systems is comparable to that at RT. Furthermore, the maximum improvements in the impact strength at RT and 77 K are, respectively, 20.3 and 26.3 % over those of the pure epoxy resin by the introduction of 10 wt.% H30.

Charpy impact testing of the DGEBF epoxy matrix cured with DETD and the MWCNT/epoxy nanocomposites is conducted at both RT and 77 K and the results are shown in Table 2.8. It can be seen that the introduction of MWCNTs at appropriate contents into epoxy resin can effectively enhance the impact strength of the epoxy resin. When the CNT content is equal to 0.5 wt.%, the impact strength is largely enhanced by 76.7 % and 51.4 % at RT and 77 K, respectively. This can be explained in terms of the synthetic sequence. Since MWCNTs are first mixed with DGEBF and the resulting mixture is then blended with the DETD with an amine

Table 2.7 Impact strength at RT and 77 K of unmodified and H30-modified epoxy resins [24]

Boltorn H30 content (wt.%)	Impact strength (kJ/m ²)	
	RT	77 K
0	25.9 ± 3.2	25.4 ± 2.7
5	27.1 ± 3.3	29.1 ± 3.3
10	31.2 ± 2.7	32.0 ± 1.0
15	24.9 ± 1.6	27.3 ± 1.4

Table 2.8 Impact strength at RT and 77 K of the epoxy matrix and epoxy nanocomposites [6]

MWCNT content (wt.%)	Impact strength (kJ/m ²)	
	RT	77 K
0	37.8 ± 3.5	24.0 ± 2.3
0.02	38.7 ± 2.5	30.9 ± 2.3
0.05	39.6 ± 3.2	31.5 ± 2.7
0.2	41.4 ± 1.6	32.4 ± 4.3
0.5	49.5 ± 4.5	35.6 ± 1.9
1	42.9 ± 0.9	26.3 ± 3.7
2	40.0 ± 1.4	22.9 ± 1.6

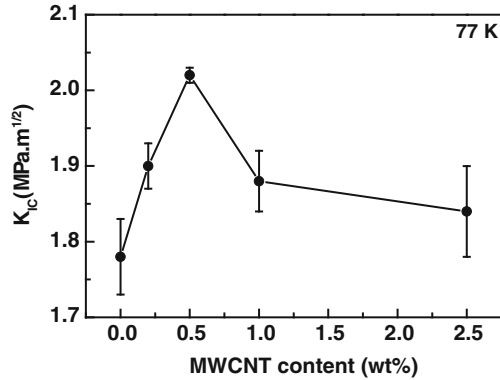
weight equivalence of 44.5 g/mol (DETD) as the curing agent and a reactive aliphatic diluent (DILUENT) as a modifier. Because the brittle DGEBF phase can be effectively toughened by introduction of CNTs, the impact strength can be significantly enhanced by the addition of CNTs at appropriate contents when no aggregates of CNTs occur. Also, Table 2.8 shows that the impact strength is larger at RT than at 77 K with the same composition. This is because the molecular mobility of the epoxy matrix would be lowered when the temperature is down to 77 K from RT. When rapid impact loading is applied to the epoxy samples, it would be difficult to yield plastic deformation and hence relatively low impact energies are required to break the samples at 77 K.

The cryogenic critical stress intensity factor (K_{IC}) for the MWCNT/PES-modified DGEBF epoxy composites is investigated as a function of CNT content [25]. Figure 2.13 shows that the fracture toughness increases with increasing the MWCNT content up to 0.5 wt.%. The maximum K_{IC} reaches 2.02 MPa m^{1/2} with an improvement of 13.5 % at 0.5 wt.% MWCNT content from 1.78 MPa m^{1/2} of the PES-modified epoxy matrix. Although the K_{IC} at 77 K of MWCNT/PES-modified epoxy composites is decreased by the further increase of MWCNT content to 1.0 and 2.5 wt.%, it is still higher than that of the epoxy matrix.

2.4 Cryogenic Thermal Properties

In cryogenic engineering technologies, the thermal properties are very important parameters for polymers. Thermal conductivity plays a significant role in the processing of cooling and heating of cryogenic devices and systems. Values for thermal expansion are required for evaluating thermally induced stresses when different materials with different thermal expansion behaviors are combined.

Fig. 2.13 Fracture toughness K_{IC} at 77 K of MWCNT/PES-modified epoxy composites [25]



Generally speaking, the thermal conductivity of polymeric materials is low when compared to other materials such as metals and ceramics. The thermal conductivity of nonconductive polymeric materials is due to the propagation of the thermal oscillation of atoms and molecules as a lattice wave (sound wave) in the material [3, 26]. Some methods have been taken to account for the temperature dependence of thermal conductivity for polymers [26–29]. The thermal conductivity is shown in Fig. 2.14 as a function of temperature for poly(methyl methacrylate) [30]. And this thermal conductivity behavior is regarded to be probably common for amorphous polymers. In the region A of very low temperature, thermal conductivity decreases roughly in terms of T^2 . In the region B of around 10 K, thermal conductivity is weakly temperature-dependent (namely a plateau region). In the region C of relatively high temperature, thermal conductivity decreases slowly with decreasing temperature.

For crystalline polymers at cryogenic temperatures, the thermal conductivity depends strongly on both crystallinity and temperature [30]. For highly crystalline polymers such as high density polyethylene, the thermal conductivity first increases with increasing temperature and then reaches a maximum near 100 K. For polymers with low crystallinity, the thermal conductivity increases slowly up to the glass transition temperature. At cryogenic temperatures, a phonon scattering mechanism arising from an acoustic mismatch at the interface between the amorphous and crystalline phase is very important. For amorphous polymers e.g., the case of poly(ethylene terephthalate), its cryogenic thermal conductivity at 1.5 K is about ten times higher than that of a partially crystalline sample [30].

Results for coefficient of thermal expansion (CTE) of seven epoxy resins are measured and presented in Fig. 2.15 [31]. Epoxy resins A, B, and C are mold resins used for cryogenic components (A: novolac, B: cycloaliphatic, and C: bisphenol A). Epoxy resins D and E are room temperature-cured epoxy resins with low thermal expansions. Resin D contains 42 wt.% calcium silicate fillers, and resin E contains 46 wt.% alumina fillers. Epoxy resins F and G are heat-resistant epoxy resins. The pure epoxy resins (A–C) exhibit higher CTE than the epoxy composites (D and E) containing inorganic particles. Moreover, the CTE for all resins decreases with decreasing the temperature.

Fig. 2.14 Temperature dependence of thermal conductivity for atactic poly (methyl methacrylate) [30]

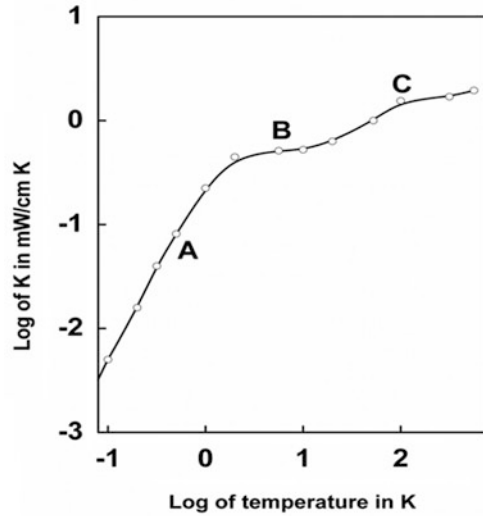
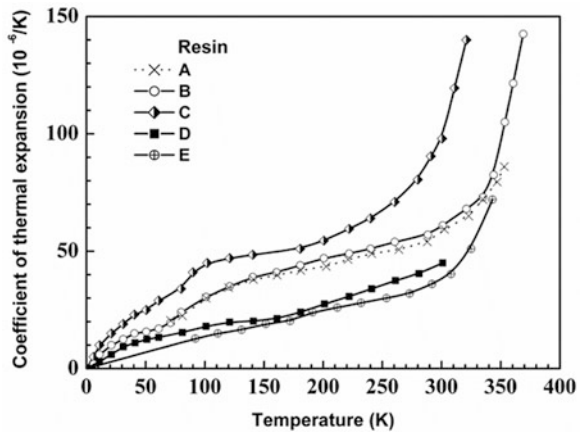


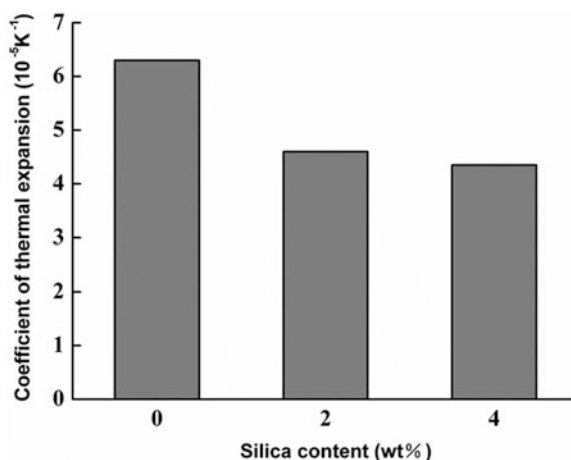
Fig. 2.15 Relationship between temperature and coefficient of thermal expansion (CTE) for the resins A–E [31]



The reduction in the CTE of polymers is desired for cryogenic applications since the CTE of polymers is normally higher than those for metals and ceramics, etc., used in cryogenic environments. The addition of silica nanoparticles can lead to the decrease in the CTE of epoxy resins. Figure 2.16 shows the average CTE from RT to 77 K of the silica/epoxy nanocomposites as a function of silica content [32]. It can be seen that the introduction of silica nanoparticles dramatically reduces the CTE. This is because silica nanoparticles have much lower CTE than epoxy resins do.

The $\Delta L/L_0$ values of silica/PI composite films with different SiO_2 weight fractions (0, 1, 3, 5, 8, 10, and 15 %) are shown in Fig. 2.17 as a function of temperature [33]. The data are fitted by least-square method and seven $\Delta L/L_0 \sim T$

Fig. 2.16 The effect of silica nanoparticle content on the average CTE from RT to 77 K [32]



curves are obtained. The differential CTE of SiO_2/PI composite films can be obtained from Fig. 2.17, and the values are shown in Fig. 2.18 and partly shown in Table 2.9.

It can be seen from Fig. 2.18 and Table 2.9 that there is an obvious effect of SiO_2 content on the CTE of SiO_2/PI composite films. The differential composite CTE decreases with decreasing testing temperature. Moreover, the CTE increases with increasing the SiO_2 content. For example, the CTE at RT decreases from $49.9 \times 10^{-6}/^\circ\text{C}$ for the pure PI film to $25.4 \times 10^{-6}/^\circ\text{C}$ for the composite film with 8 wt.% silica. Also, when the SiO_2 content reaches to 15 wt.%, the differential CTE corresponds to the lowest values. The morphology study [34, 35] shows that the particles are well dispersed in the polyimide matrix and the mean particle size decreases dramatically as the silica content decreases. Combination of the morphological observation and the results for the CTE indicates that the silica particle size has a much less effect on the CTE but the particle content shows a relatively significant effect on the CTE.

2.5 Cryogenic Creep and Sliding Performance

Cryogenic creep fracture of the polymers is the probable cause of the delayed coil quenching in superconductive technology. Research on friction property of polymers and composites at low temperatures is attributed to the application of superconducting magnetic winding systems.

The creep strains, etc., at 77 K in epoxy resins B, E, and G under a compressive stress of -100 MPa are shown in Fig. 2.19 [31]. It is shown that epoxy resins exhibit large creep deformations even under elastic deformation at a cryogenic temperature. The cryogenic creep strains are in typical stage-I logarithmic creep, in which the strain hardening mechanism is dominant. The creep strains are almost

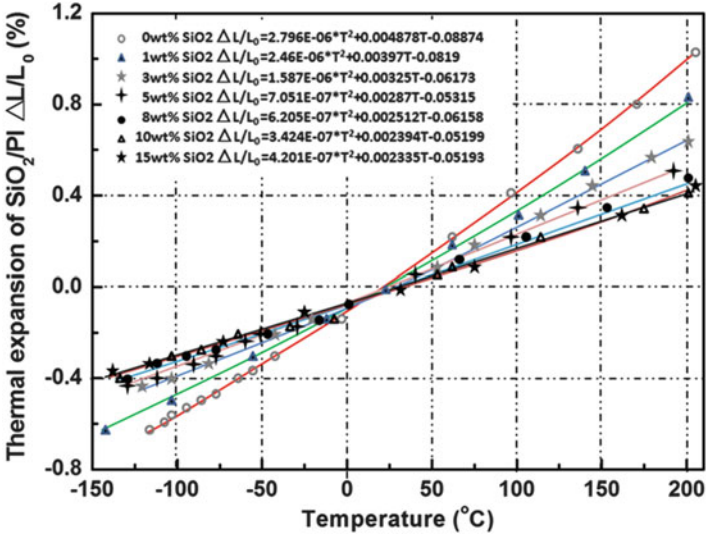


Fig. 2.17 Thermal expansion of silica/polyimide (PI) composite films [33]

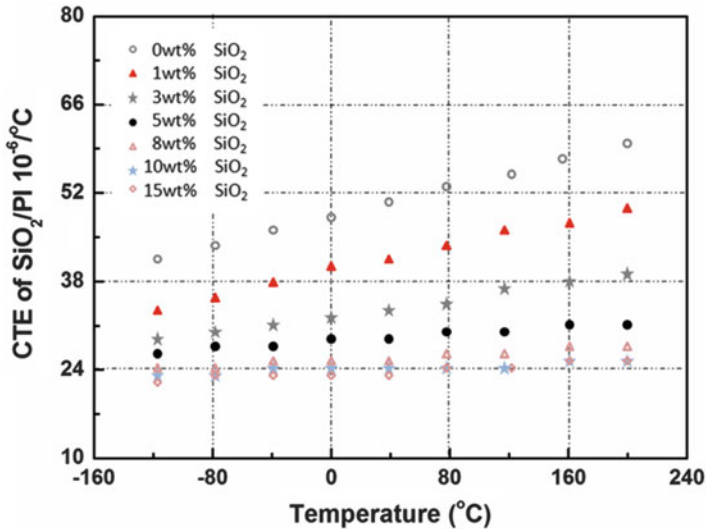


Fig. 2.18 Differential CTE of silica/PI composite films [33]

proportional to the logarithmic time after about 10^3 s. Extrapolation displays that the creep strains at 3×10^8 s can be evaluated as twice as those at 10^5 s. This type of cryogenic creep deformation may cause a delayed resin fracture at an operating temperature. Figure 2.19 also shows the results for the recovery strains after the unloading. The recovery strains are similar to or larger than the creep strains up to

Table 2.9 Differential CTE of SiO₂/PI films calculated from Fig. 2.17 at three typical temperatures for the 0–15 wt.% silica content [33]

<i>T</i> (°C)	CTE (10 ^{−6} /°C)						
	0 wt.%	1 wt.%	3 wt.%	5 wt.%	8 wt.%	10 wt.%	15 wt.%
−100	43.2	34.8	29.3	27.2	23.9	23.3	22.5
20	49.9	40.7	33.1	29.0	25.4	24.1	23.5
200	60.0	49.5	38.9	31.7	27.6	25.3	25.0

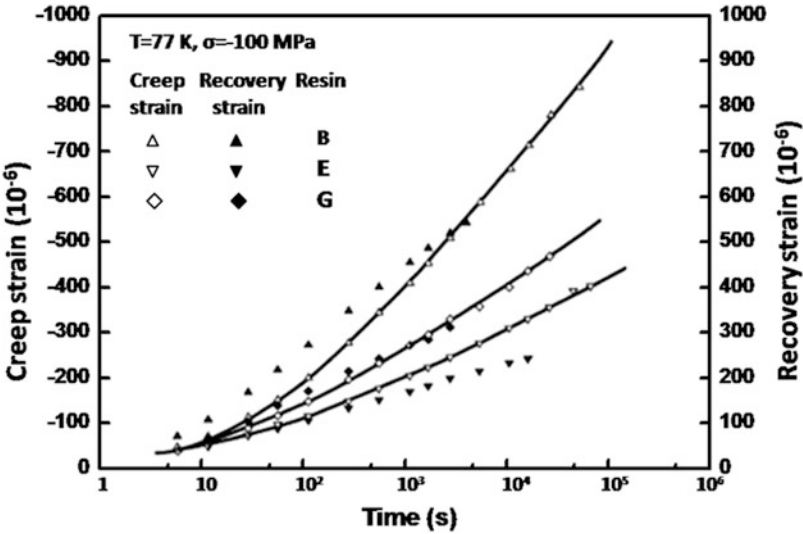


Fig. 2.19 Creep and recovery strains under -100 MPa at 77 K in resins B, E, and G mentioned in Fig. 2.14 [31]

10^3 s . When the load is applied again after recovery, creep deformation will occur, similar to that at the first loading.

Details and frictional property of some polymer composites are shown in Table 2.10 and Fig. 2.20 [36]. The average diameter of short carbon fibers is approximately $14.5\text{ }\mu\text{m}$, with an average fiber length of about $90\text{ }\mu\text{m}$. The particle size of polytetrafluoroethylene (PTFE) is around $4\text{ }\mu\text{m}$, whereas that of the graphite flakes is around $20\text{ }\mu\text{m}$. TiO₂ (Kronos 2310) with an average diameter of 300 nm is applied as an additional nano-size filler. Figure 2.20 gives the results for the friction coefficient of some composites based on different polymers as a function of temperature. It is observed that the friction coefficient of all composites is reduced with lowering the testing temperature. There are two possible reasons for the reduction in frictional coefficient: (1) the increase of stiffness of the polymer composites at low temperatures; and (2) the liquid lubricating effect of the cryogenic media (either liquid nitrogen or liquid hydrogen) between the two contact partners.

Table 2.10 Details of composites based on various polymer matrices [36]

Matrix	Short carbon fiber (vol.%)	Graphite (vol)	PTFE (vol.%)	TiO ₂ (300 nm) (vol.%)
Epoxy	15	15	0	5
Polyetheretherketone (PEEK)	15	5	5	0
Polyamide 6,6 (PA 6,6)	15	5	0	5
Polyetherimide (PEI)	5	15	0	5

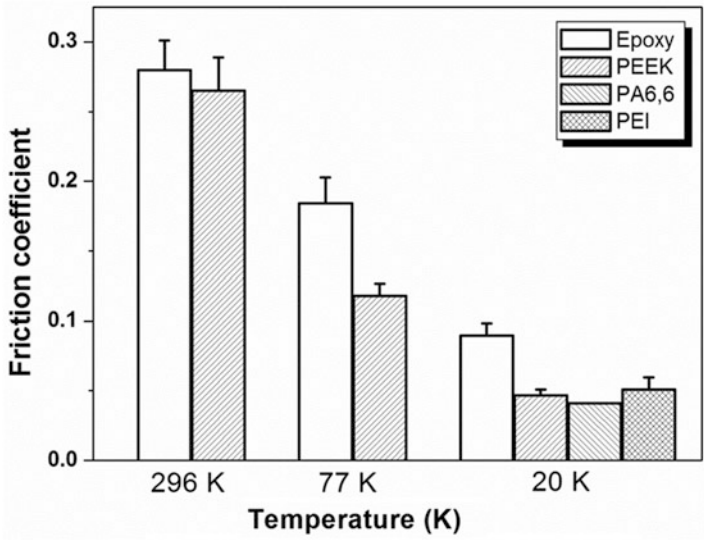


Fig. 2.20 Friction coefficient of different matrix composites in liquid hydrogen (20 K) and liquid nitrogen (77 K) [36]

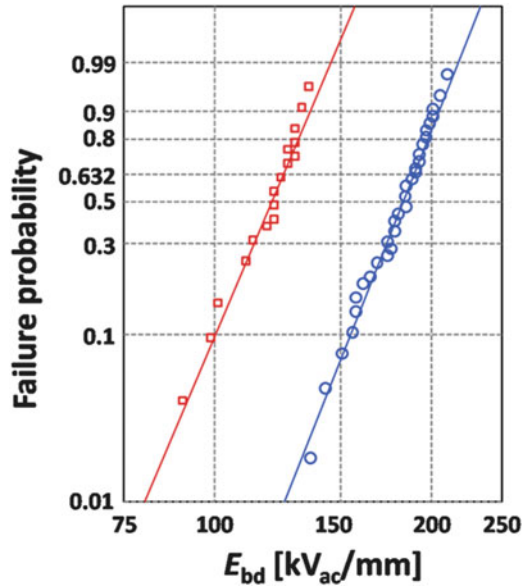
2.6 Cryogenic Dielectric Properties

It is scarcely seen materials specially designed for cryogenic dielectric applications utilizing high-temperature superconductors (HTSs). So, electrical insulation materials used in conventional high voltage and nonconducting structural materials are adapted as cryogenic dielectric materials for HTS power applications.

The comparison of dielectric breakdown data for polyamide 6,6 (PA 6,6) and polypropylene-laminated paper (PPLP) is shown in Fig. 2.21, where E_{bd} is the dielectric breakdown field. It shows that PA 6,6 has significantly (57 %) higher breakdown strength than PPLP [37]. This means that high voltage equipment with thinner insulation can be made using PA 6,6 instead of PPLP.

TiO₂ nanoparticles with a diameter smaller than 5 nm are synthesized in situ to fabricate a cryogenic resin nanocomposite. The nanocomposite with 2.5 wt.% TiO₂ shows a uniform distribution of the particles as clusters in the epoxy matrix.

Fig. 2.21 Comparison of polyamide 6,6 (PA 6,6) dielectric breakdown data with polypropylene-laminated paper (PPLP). The data for PA 6,6 and PPLP are presented with circles (*open circle*) and (*open square*) symbols, respectively [37]. The measurements are performed in liquid nitrogen open bath at 77 K



The dielectric breakdown data of the nanocomposite show significant improvement over the pristine epoxy, as shown in Fig. 2.22. The data are presented in terms of Weibull statistics [39, 40]

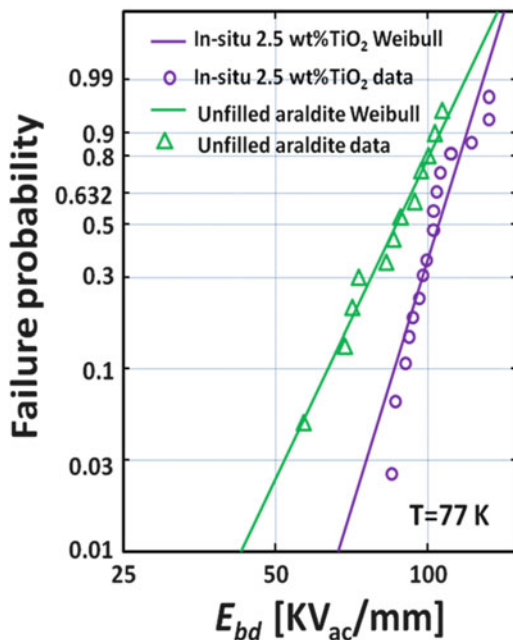
$$P(\alpha, \beta, E_{bd}) = 1 - \exp[-(E_{bd}/\alpha)^\beta] \quad (2.1)$$

where E_{bd} is the dielectric breakdown field, α the characteristic breakdown strength at which the failure probability $P = 0.6321$, and β the slope which corresponds to inverse scattering in the breakdown values. The parameters α and β are estimated, respectively, as 93.4 kV/mm and 5.98 for the pristine epoxy resin, whereas the nanocomposite shows 109.9 kV/mm and 9.48 for α and β . The improvement in the characteristic breakdown strength is approximately equal to 20 % due to 60 % improvement in the slope. Finally, a possible dielectric design parameter can be adopted by using (2.1) as the 1 % failure probability field, which is 56 % higher in the nanocomposite (67.7 kV/mm) than in the unfilled epoxy resin (43.3 kV/mm). This improvement means 0.64 times less insulation thickness for a given voltage level.

2.7 Influence of Water Absorption and Cryogenic Aging on Cryogenic Properties

Polymers may absorb some amount of water and serve under cryogenic thermal cycling. Effects of water absorption and cryogenic aging on cryogenic properties are briefly summarized below.

Fig. 2.22 The dielectric breakdown failure probability data measured with 500 V/s at a power frequency of 60 Hz at 77 K [38]. The *solid lines* correspond to estimates from a Weibull statistical analysis

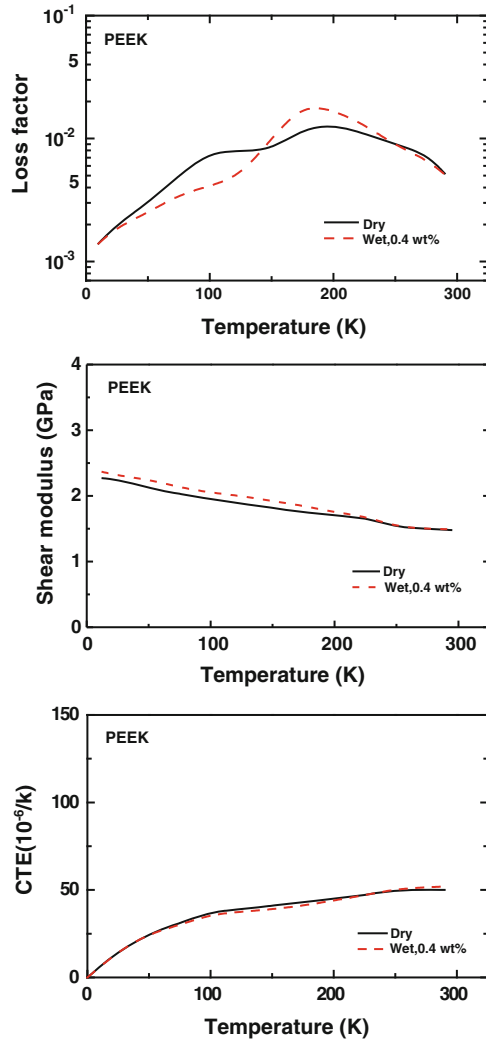


The results for the loss factor ($\tan\delta$), the shear modulus (G), and the CTE (α) are presented in Figs. 2.23 and 2.24, respectively, for semicrystalline polyetheretherketone (PEEK) and polyethersulphone (PES), which are in the dry and nearly water-saturated state. It can be seen from Fig. 2.23 that the shear modulus of PEEK is increased below the water peak at around 170 K, the damping peak at very low temperatures is suppressed by water absorption, and nearly no influence on the CTE is observed below 320 K.

The influence of water absorption on the cryogenic properties of PES is similar. One reason might be that water is attached to a different polar group (sulphone group). As is seen from Fig. 2.24, the existing damping peak at 175 K is increased only slightly while the shear modulus is increased remarkably below 170 K. This is also true for the Young's modulus shown in Table 2.11, in which the results for the Young's modulus, E , are given. A slight reduction of E_{wet} at RT and a slight increase of E_{wet} at 77 K can be observed. However, the shear modulus is much less influenced by water above 200 K. Moreover, there is only a slight influence of water on the thermal expansion of PES. Below around 180 K, the thermal expansion is reduced by water while above 180 K, the CTE is increased by water.

The situation is somewhat different for polyamides, which are nonaromatic and have a low main glass transition temperature. No damping peaks exist at very low temperatures and no influence of water is observed below 140 K at low water concentrations as seen in Fig. 2.25 for PA 12 [41]. A small increase in shear modulus due to water is observed in the temperature region starting at around 140 K. Below that temperature no shear modulus increase is observed. A shear modulus decrease by water (softening effect), however, starts above 280 K.

Fig. 2.23 Loss factor, shear modulus, and thermal expansion of dry and wet PEEK [41]



This may be the influence of the main glass transition whose tail can be seen from the damping spectra above 300 K. In Table 2.11, the Young's modulus of PA 12 is given for the dry and wet samples. The Young's modulus at RT is reduced by water while that at 77 K is almost not influenced by water. In addition, at a temperature below around 80 K, the effect of water on the thermal expansion of PA 12 can be neglected while above around 80 K the thermal expansion is reduced by water.

Two grades of solvent-cast polyarylate films manufactured by ISONOVA, namely 15F and 25F with thicknesses of 120 and 100 μm , respectively, are selected for investigation of the cryogenic aging treatment on their properties [42]. Electrical and mechanical properties of some polymers are studied by considering

Fig. 2.24 Loss factor, shear modulus, and thermal expansion of dry and wet PES [41]

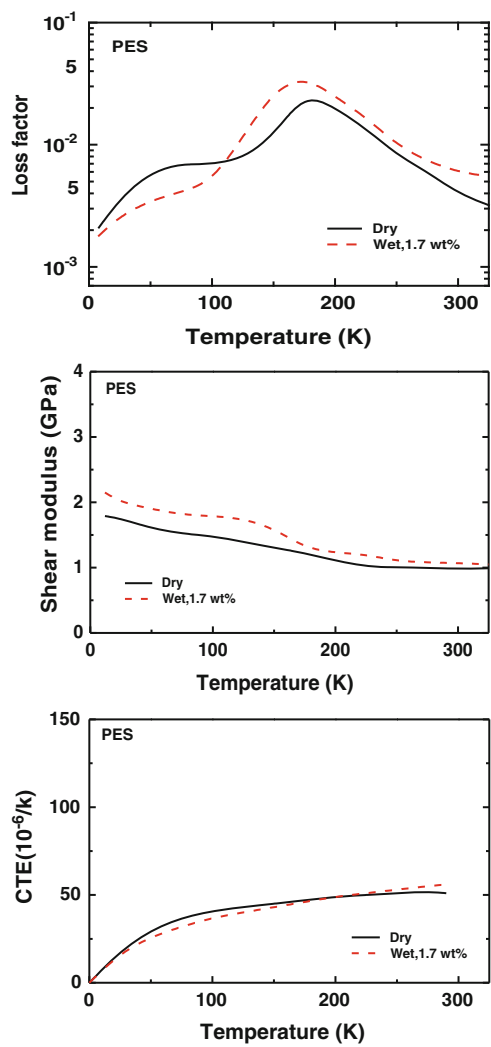
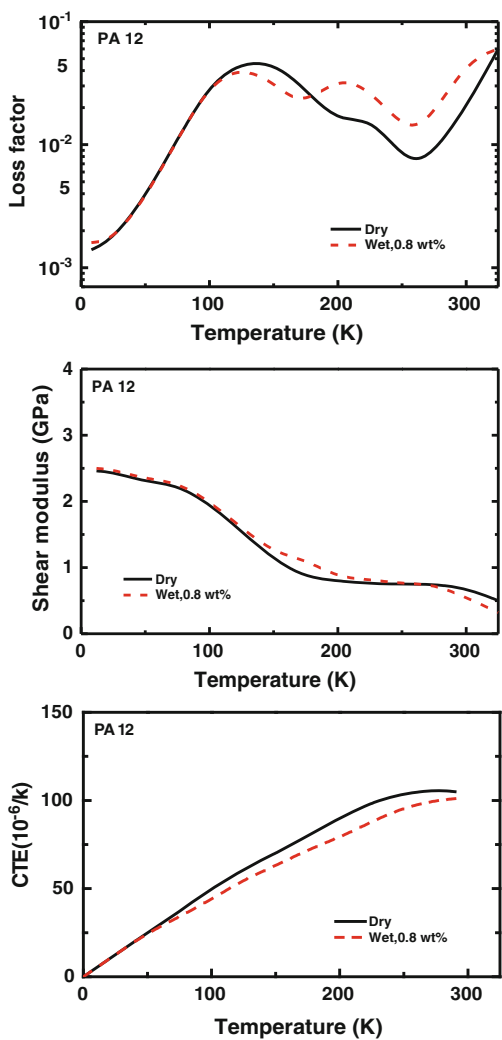


Table 2.11 Elastic modulus of dry and wet PES and PA12 samples [41]

Testing temperature	PES		PA 12	
	E_{dry}	E_{wet} (1.4 wt.% water)	E_{dry}	E_{wet} (0.4 wt.% water)
RT (GPa)	2.83	2.70	2.05	1.83
77 K (GPa)	4.58	5.66	6.65	6.70

cryogenic aging treatment like soaking in liquid nitrogen for 24 h [42]. Table 2.12 shows the volume and surface resistance of the polymer films measured by applying a d.c. potential of 500 V and a circular size sample of 6 cm in diameter. The cryogenic aging seems to have no significant influence on resistance in the

Fig. 2.25 Loss factor, shear modulus, and thermal expansion of dry and wet PA 12 [41]



experimental error range. The only appreciable change is observed in the increase of surface resistance of aged 25F film. This behavior is regarded to result from surface preparation and contamination.

Table 2.12 also shows the results for the mechanical properties of control and aged samples. The tensile strength and elongation at break does not change much with cryogenic aging. The Young’s modulus appears to exhibit a slight increase for both aged films. In summary, it seems that the cryogenic aging does not have a significant influence on the tensile properties.

Table 2.12 Volume and surface resistivity, and mechanical properties of polyarylate films [42]

Property	Grade 15F		Grade 25F	
	Control	Aged	Control	Aged
Volume resistance (Ω cm)	1.1×10^{16}	5.5×10^{15}	6.2×10^{15}	7.6×10^{15}
Surface resistance (Ω)	9.2×10^{13}	1.3×10^{14}	6.3×10^{13}	1.1×10^{17}
Tensile strength (MPa)	81	80	74	76
Young's modulus (GPa)	0.80	0.91	1.04	1.06
Elongation at break (%)	82	76	47	48

2.8 Concluding Remarks and Outlooks

With the new developments of space, superconducting, electronic and defense technologies as well as large cryogenic engineering projects such as International Thermonuclear Experimental Reactor (ITER), etc., polymers are increasingly applied as electrical insulators, thermal insulators, vacuum sealants, and matrix materials for composites, etc., used in cryogenic environments. And the polymers need to withstand exerted load by applied magnetic field, etc., severe cryogenic environment and thermal cycling. The cryogenic mechanical and physical properties of polymers are thus critical parameters for determining the applicability of polymers for use in the severe cryogenic environments. The cryogenic properties studied previously include tensile strength, modulus, elongation at break, fracture resistance, thermal conductivity, thermal expansion, shear strength, and dielectric breakdown strength, etc. Some attempt is also made to examine the effects of water absorption and cryogenic aging, etc., on the cryogenic properties of polymers. The previous knowledge on cryogenic properties of polymers provides useful information and strong evidence that can tell us what polymers may be employed in cryogenic engineering applications.

So far there are only a limited number of polymers successfully used in cryogenic engineering areas possibly because the cryogenic mechanical and physical properties of most polymers are low and cannot meet the requirements by the cryogenic engineering applications. Modification of polymers is possibly a good means to enhance their cryogenic properties. However, relatively little work has been reported on modification of polymers using modifiers to enhance the cryogenic properties of polymers so that the modified polymers may meet the high requirements by the cryogenic engineering applications. Moreover, very little work is made on hybridization of polymers using multifunctional fillers to get multifunctional composites for cryogenic applications. Therefore, future research work should be extensively directed towards enhancements of cryogenic properties of polymers by modifying methods so that modified polymers will receive greater success in their applications in cryogenic engineering areas. Multifunctional composites are also an important direction for future work in this subject so that polymers can be successfully applied in multifunctional devices such as cryogenic sensors and actuators, etc., used in cryogenic environments.

Acknowledgements This work was financially supported by the National Natural Science Foundation of China (Nos. 10672161, 50573090, 10972216, 51073169, and 11002142), the National Basic Research Program of China (No. 2010CB934500), Key Research Program of Beijing City Science and Technology Committee (No H020420020230), and the Overseas Outstanding Scholar Foundation of the Chinese Academy of Sciences (Nos. 2005-1-3 and 2005-2-1).

References

1. Nobelen M, Hayes BS, Seferis JC (2003) Cryogenic microcracking of rubber toughened composites. *Polym Compos* 24(6):723–730. doi:[10.1002/pc.10066](https://doi.org/10.1002/pc.10066)
2. Ueki T, Nishijima S, Izumi Y (2005) Designing of epoxy resin systems for cryogenic use. *Cryogenics* 45(2):141–148. doi:[10.1016/j.cryogenics.2004.07.002](https://doi.org/10.1016/j.cryogenics.2004.07.002)
3. Yano O, Yamaoka H (1995) Cryogenic properties of polymers. *Prog Polym Sci* 20(4):585–613. doi:[10.1016/0079-6700\(95\)00003-X](https://doi.org/10.1016/0079-6700(95)00003-X)
4. Nishino T, Okamoto T, Sakurai H (2011) Cryogenic mechanical behavior of poly(trimethylene terephthalate). *Macromolecules* 44(7):2106–2111. doi:[10.1021/ma200111v](https://doi.org/10.1021/ma200111v)
5. Zhang YH, Wu JT, Fu SY, Yang SY, Li Y, Fan L, Li RKY, Li LF, Yan Q (2004) Studies on characterization and cryogenic mechanical properties of polyimide-layered silicate nanocomposite films. *Polymer* 45(22):7579–7587. doi:[10.1016/j.polymer.2004.08.032](https://doi.org/10.1016/j.polymer.2004.08.032)
6. Chen ZK, Yang JP, Ni QQ, Fu SY, Huang YG (2009) Reinforcement of epoxy resins with multi-walled carbon nanotubes for enhancing cryogenic mechanical properties. *Polymer* 50(19):4753–4759. doi:[10.1016/j.polymer.2009.08.001](https://doi.org/10.1016/j.polymer.2009.08.001)
7. Basara G, Yilmazer U, Bayram G (2005) Synthesis and characterization of epoxy based nanocomposites. *J Appl Polym Sci* 98(3):1081–1086. doi:[10.1002/app.22242](https://doi.org/10.1002/app.22242)
8. Rosso P, Friedrich K, Wollny A (2002) Evaluation of the adhesion quality between differently treated carbon fibers and an in-situ polymerized polyamide 12 system. *J Macromol Sci B41* (4–6):745–759. doi:[10.1081/MB-120013062](https://doi.org/10.1081/MB-120013062)
9. Fu SY, Feng XQ, Lauke B, Mai YW (2008) Effects of particle size, particle/matrix interface adhesion and particle loading on mechanical properties of particulate-polymer composites. *Compos Part B Eng* 39(6):933–961. doi:[10.1016/j.compositesb.2008.01.002](https://doi.org/10.1016/j.compositesb.2008.01.002)
10. Fu SY, Lauke B (1998) An analytical characterization of the anisotropy of the elastic modulus of misaligned short-fiber-reinforced polymers. *Compos Sci Technol* 58(12):1961–1972. doi:[10.1016/S0266-3538\(98\)00033-5](https://doi.org/10.1016/S0266-3538(98)00033-5)
11. Fu SY, Lauke B (1998) The elastic modulus of misaligned short-fiber-reinforced polymers. *Compos Sci Technol* 58(3–4):389–400. doi:[10.1016/S0266-3538\(97\)00129-2](https://doi.org/10.1016/S0266-3538(97)00129-2)
12. Chen ZK, Yang G, Yang JP, Fu SY, Ye L, Huang YG (2009) Simultaneously increasing cryogenic strength, ductility and impact resistance of epoxy resins modified by n-butyl glycidyl ether. *Polymer* 50(5):1316–1323. doi:[10.1016/j.polymer.2008.12.048](https://doi.org/10.1016/j.polymer.2008.12.048)
13. Yang JP, Yang G, Xu GS, Fu SY (2007) Cryogenic mechanical behaviors of MMT/epoxy nanocomposites. *Compos Sci Technol* 67(14):2934–2940. doi:[10.1016/j.compscitech.2007.05.012](https://doi.org/10.1016/j.compscitech.2007.05.012)
14. Deng YM, Gu AJ, Fang ZP (2004) The effect of morphology on the optical properties of transparent epoxy/montmorillonite composites. *Polym Int* 53(1):85–91. doi:[10.1002/pi.1410](https://doi.org/10.1002/pi.1410)
15. Shindo Y, Kuronuma Y, Takeda T, Narita F, Fu SY (2012) Electrical resistance change and crack behavior in carbon nanotube/polymer composites under tensile loading. *Compos Part B Eng* 43(1):39–43. doi:[10.1016/j.compositesb.2011.04.028](https://doi.org/10.1016/j.compositesb.2011.04.028)
16. Takeda T, Shindo Y, Narita F, Mito Y (2009) Tensile characterization of carbon nanotube-reinforced polymer composites at cryogenic temperatures: experiments and multiscale simulations. *Mater Trans* 50(3):436–445. doi:[10.2320/matertrans.MBW200817](https://doi.org/10.2320/matertrans.MBW200817)

17. Thostenson ET, Chou TW (2006) Carbon nanotube networks: sensing of distributed strain and damage for life prediction and self healing. *Adv Mater* 18(21):2837–2841. doi:[10.1002/adma.200600977](https://doi.org/10.1002/adma.200600977)
18. Chen Q, Gao BJ, Chen JL (2003) Properties of impregnation resin added to multifunctional epoxy at cryogenic temperature. *J Appl Polym Sci* 89(5):1385–1389. doi:[10.1002/app.12431](https://doi.org/10.1002/app.12431)
19. Hu XL, Huang PC (2005) Influence of polyether chain and synergetic effect of mixed resins with different functionality on adhesion properties of epoxy adhesives. *Int J Adhes Adhes* 25(4):96–300. doi:[10.1016/j.ijadhdh.2004.08.001](https://doi.org/10.1016/j.ijadhdh.2004.08.001)
20. Pavlick MM, Johnson WS, Jensen B, Weiser E (2009) Evaluation of mechanical properties of advanced polymers for composite cryotank applications. *Compos Part A Appl Sci* 40(4):359–367. doi:[10.1016/j.compositesa.2008.12.009](https://doi.org/10.1016/j.compositesa.2008.12.009)
21. Yang G, Zheng B, Yang JP, Xu GS, Fu SY (2008) Preparation and cryogenic mechanical properties of epoxy resins modified by poly(ethersulfone). *J Polym Sci A Polym Chem* 46(2):612–624. doi:[10.1002/pola.22409d](https://doi.org/10.1002/pola.22409d)
22. McGarry FJ (1970) Building design with fibre reinforced materials. *Proc R Soc Lond Ser A* 319(1536):59. doi:[10.1098/rspa.1970.0165](https://doi.org/10.1098/rspa.1970.0165)
23. Kinloch AJ, Young RJ (1989) Fracture behaviour of polymers. Applied Science, New York
24. Yang JP, Chen ZK, Yang G, Fu SY, Ye L (2008) Simultaneous improvements in the cryogenic tensile strength, ductility and impact strength of epoxy resins by a hyperbranched polymer. *Polymer* 49(13–14):3168–3175. doi:[10.1016/j.polymer.2008.05.008](https://doi.org/10.1016/j.polymer.2008.05.008)
25. Yang JP, Chen ZK, Feng QP, Deng YH, Liu Y, Ni QQ, Fu SY (2012) Cryogenic mechanical behaviors of carbon nanotube reinforced composites based on modified epoxy by poly(ethersulfone). *Compos Part B Eng* 43(1):22–26. doi:[10.1016/j.compositesb.2011.04.037](https://doi.org/10.1016/j.compositesb.2011.04.037)
26. Morgan GJ, Smith D (1974) Thermal conduction in glasses and polymers at low temperatures. *J Phys C* 7(4):649–664. doi:[10.1088/0022-3719/7/4/004](https://doi.org/10.1088/0022-3719/7/4/004)
27. Gush HP (1991) A compact low thermal-conductivity support for cryogenic use. *Rev Sci Instrum* 62(4):1106. doi:[10.1063/1.1142017](https://doi.org/10.1063/1.1142017)
28. Greig D (1988) Low temperature thermal-conductivity of polymers. *Cryogenics* 28(4):243–247. doi:[10.1016/0011-2275\(88\)90008-2](https://doi.org/10.1016/0011-2275(88)90008-2)
29. Nittke A, Scherl M, Esquinazi P, Lorenz W, Li JY, Pobell F (1995) Low-temperature heat release, sound-velocity and attenuation, specific-heat and thermal conductivity in polymers. *J Low Temp Phys* 98(5–6):517–547. doi:[10.1007/BF00752280](https://doi.org/10.1007/BF00752280)
30. Choy CL (1977) Thermal-conductivity of polymers. *Polymer* 8(10):984–1004. doi:[10.1016/0032-3861\(77\)90002-7](https://doi.org/10.1016/0032-3861(77)90002-7)
31. Usami S, Ejima H, Suzuki T, Asano K (1999) Cryogenic small-flaw strength and creep deformation of epoxy resins. *Cryogenics* 39(9):729–738. doi:[10.1016/S0011-2275\(99\)00084-3](https://doi.org/10.1016/S0011-2275(99)00084-3)
32. Huang CJ, Fu SY, Zhang YH, Lauke B, Li LF, Ye L (2005) Cryogenic properties of SiO₂/epoxy nanocomposites. *Cryogenics* 45(6):450–454. doi:[10.1016/j.cryogenics.2005.03.003](https://doi.org/10.1016/j.cryogenics.2005.03.003)
33. Chen XG, Guo JD, Zheng B, Li YQ, Fu SY, He GH (2007) Investigation of thermal expansion of PI/SiO₂ composite films by CCD imaging technique from -120 to 200 °C. *Compos Sci Technol* 67(14):3006–3013. doi:[10.1016/j.compscitech.2007.05.029](https://doi.org/10.1016/j.compscitech.2007.05.029)
34. Li Y, Fu SY, Li YQ, Pan QY, Xu GS, Yu CY (2007) Improvements in transmittance, mechanical properties and thermal stability of silica-polyimide composite films by a novel sol-gel route. *Compos Sci Technol* 67(11–12):2408–2416. doi:[10.1016/j.compscitech.2007.01.003](https://doi.org/10.1016/j.compscitech.2007.01.003)
35. Zhang YH, Li Y, Fu SY, Xin JH, Daoud WA, Li LF (2005) Synthesis and cryogenic properties of polyimide–silica hybrid films by sol–gel process. *Polymer* 46(19):8373–8380. doi:[10.1016/j.polymer.2005.07.012](https://doi.org/10.1016/j.polymer.2005.07.012)
36. Zhang Z, Klein P, Theiler G, Huebner W (2004) Sliding performance of polymer composites in liquid hydrogen and liquid nitrogen. *J Mater Sci* 39(9):2989–2995. doi:[10.1023/B:JMSC.0000025824.18291.f0](https://doi.org/10.1023/B:JMSC.0000025824.18291.f0)
37. Tuncer E, Polizos G, Sauers I, James DR, Ellis AR, Messman JM, Aytug T (2009) Polyamide 66 as a cryogenic dielectric. *Cryogenics* 49(9):463–468. doi:[10.1016/j.cryogenics.2009.06.008](https://doi.org/10.1016/j.cryogenics.2009.06.008)
38. Polizos G, Tuncer E, Sauers I, More KL (2010) Properties of a nanodielectric cryogenic resin. *Appl Phys Lett* 96(15):152903. doi:[10.1063/1.3394011](https://doi.org/10.1063/1.3394011)

39. Weibull W (1951) A statistical distribution of function of wide applicability. *J Appl Mech* 18 (3):293–297
40. Rowland SM, Hill RM, Dissado LA (1986) Censored Weibull statistics in the dielectric-breakdown of the oxide-films. *J Phys C Solid State Phys* 19(31):6263–6285. doi:[10.1088/0022-3719/19/31/020](https://doi.org/10.1088/0022-3719/19/31/020)
41. Baschek G, Hartwig G, Zahradnik F (1999) Effect of water absorption in polymers at low and high temperatures. *Polymer* 40(12):3433–3441. doi:[10.1016/S0032-3861\(98\)00560-6](https://doi.org/10.1016/S0032-3861(98)00560-6)
42. Patterson RL, Hammoud A, Fialla P (2002) Preliminary evaluation of polyarylate dielectric films for cryogenic applications. *J Mater Sci Mater Electron* 13(6):363–365. doi:[10.1023/A:1015656700768](https://doi.org/10.1023/A:1015656700768)

Polymers at Cryogenic Temperatures

Kalia, S.; Fu, S.-Y. (Eds.)

2013, VIII, 292 p., Hardcover

ISBN: 978-3-642-35334-5